On the Effect of Wave Direction on Control and Performance of a Moored Pitching Wave Energy Conversion System

Journal of
Marine Science and Engineering

MDPI

Article

On the Effect of Wave Direction on Control and Performance of a Moored Pitching Wave Energy Conversion System

Bruno Paduano *, Nicolás Faedo and Giuliana Mattiazzo

Marine Offshore Renewable Energy Lab, Politecnico di Torino, 10128 Turin, Italy; nicolas.faedo@polito.it (N.F.); giuliana.mattiazzo@polito.it (G.M.)
* Correspondence: bruno.paduano@polito.it

Abstract: In the pathways towards the commercialisation of wave energy systems, the need for reliable mathematical models is of paramount importance for the design and synthesis of model-based control techniques to maximise the performance of wave energy converters (WECs). Furthermore, these offshore marine systems are held in position by the use of mooring systems, which have recently been analysed beyond survivability conditions to investigate their influence on control synthesis and device performance. In this study, we delve into the complex challenge of incorporating relevant mooring dynamics in defining a representative control action while also examining the influence of wave directionality on the overall procedure. For the specific case of a spread mooring system, where the hull cannot weathervane and operates based on directionality, control synthesis must be performed taking into account this characteristic of the resource. In this context, because it is able to harvest energy from only the bow-directed waves, the PeWEC is considered as a representative case study. The control synthesis is realised using a tailored data-based model, and device performance is evaluated across different site conditions while accounting for wave direction. Among our overall conclusions, we show that neglecting the directionality of the wave resource for the PeWEC case study can lead to an overestimation of device performance of up to 50%, even though a prevalent wave direction exists at the site.

Keywords: wave energy; pitching device; PeWEC; moorings; productivity; performances; control; data-based model

Citation: Paduano, B.; Faedo, N.; Mattiazzo, G. On the Effect of Wave Direction on Control and Performance of a Moored Pitching Wave Energy Conversion System. *J. Mar. Sci. Eng.* **2023**, *11*, 2001. https://doi.org/10.3390/jmse11102001

Academic Editor: Eugen Rusu

Received: 13 September 2023
Revised: 8 October 2023
Accepted: 12 October 2023
Published: 17 October 2023

1. Introduction

The evolution of renewable energies has paved the way for the development of various technologies, with ocean energy still remaining largely untapped. In particular, ocean energy encompasses different harvesting methods with wave energy holding significant promise, as it possesses the second-largest energy potential [1,2]. While the ocean energy sector has made remarkable strides in recent years, it remains in its early stages, with several advanced prototypes undergoing current testing. However, the global installed capacity remains limited to just a few megawatts. The industry faces pressing challenges, including the need for further technological development to establish reliability and robustness and cost reduction, as well as overcoming deployment hurdles and mitigating risks [3–6]. Evaluating the importance of an energy source involves considering both its potential and the capacity of the available technology to extract power from it. Recent studies indicate that wave energy extraction could reach around 10–20% of its total potential [5,7–9]. This level of power extraction has the capabilities of contributing with a substantial portion of the overall energy consumption [10].

As the energy stored in a wave diminishes with increasing water depth and distance from the shore [11], most wave energy converters (WECs) are classified as offshore floating devices [12]. Consequently, these WECs require specific locations for deployment. A crucial component in ensuring the proper functioning of these devices is the mooring system, which addresses the station-keeping problem.

Compared to traditional offshore structures, like floating production storage and offloading units, wave energy technologies present more complex systems for station keeping. This complexity arises from the need to maintain the device energy extraction characteristics, i.e., minimising the effect of the mooring dynamics in operating conditions, while ensuring its structural integrity [12].

The optimisation of energy extraction typically involves employing control techniques derived from optimal control theory [13]. In wave energy systems, control actions are virtually always computed using a model-based approach [14]. Therefore, accounting for the effect of the mooring system on the overall system response becomes crucial in the process of synthesising effective and representative control actions. Designing a reliable controller necessitates a thorough understanding of the system dynamics, including the relevant mooring dynamics. However, modelling moorings accurately within a tractable WEC model is inherently challenging due to their potentially nonlinear behaviour [15], which can (at least partially) explain why the vast majority of control studies available for WEC systems do not incorporate any information on the effect of the station-keeping component. As a matter of fact, while the influence of moorings on device dynamics is acknowledged in the existing literature, the vast majority of the state-of-the-art studies in the wave energy domain primarily focus on mooring system design under survivability conditions (see, e.g., [16–18], to cite a few).

If the station-keeping system significantly influences the dynamics of WECs, synthesising control actions without considering the mooring system can lead to non-representative and suboptimal results [19–22].

Furthermore, though, in general, performance assessments omit the influence of the wave direction on the device performances [23,24], and the associated device dynamics can be significantly influenced if a directional device is investigated, (i.e., a device capable of harvesting energy from a single direction), because the mooring system reduces the device's weathervaning capabilities. In addition, it is not clear in the state of the art how the wave directionality directly influences the response of a moored system and, consequently, the definition of a representative control action.

With the intention of providing insight into wave energy systems modelling, this study expands upon the control synthesis approach proposed in [20]. In particular, we incorporate wave directionality into the analysis and the assessment of a representative wave energy system performance based on representative site conditions. Acknowledging the impact of nonlinear factors on the overall dynamics, such as mooring restoring forces and wave second-order forces, among others (see Section 3), the results are evaluated using a nonlinear numerical model. By overcoming the limitations associated with wave directionality, this study comprehensively assesses the productivity of the pendulum wave energy converter (PeWEC) across a wide spectrum of scenarios. Among the available WECs, the PeWEC has been chosen as a representative case study due to its multi-degrees-of-freedom (DoFs) nature, comprehensive PTO conversion mechanism, and the relevance of the mooring system for device station keeping and alignment.

The remainder of this study is organised as follows: In Section 2, the device under investigation is presented alongside its main characteristics, working principle, and corresponding mooring system. In Section 3, the numerical models adopted to evaluate both the data-based models and device productivity are presented. In Section 4, the control synthesis of the device is analysed and the application of such a synthesis by means of a tailored data-based model is described. Section 5 outlines the simulation process and describes the main results of the productivity analysis and, finally, in Section 6 the main findings of this study are reported.

Notation

With $\mathbb{R}^+$, the set of positive real numbers is represented. $F(\omega) = \mathcal{F}(f(t))$ represents the Fourier transform of the function f. Moreover, whenever a function is represented by a Greek letter, its Fourier transform is indicated with a *tilde*, e.g., the Fourier transform of the

η is expressed with $\tilde{\eta}$. Given a matrix $A \in \mathbb{C}^{n\times m}$, $A^* \in \mathbb{C}^{n\times m}$ represents the Hermitian of A. Additionally, given a square non-singular matrix $B \in \mathbb{C}^{n\times n}$, $B^{-*} \in \mathbb{C}^{n\times n}$ denotes the inverse Hermitian of B. Considering $A \in \mathbb{C}^{n\times m}$, $\{\Re(A), \Im(A)\} \subset \mathbb{R}^{n\times m}$ represents the real and the imaginary parts of the matrix A, respectively.

2. The PeWEC Case

With the purpose of keeping this paper reasonably self-contained, a brief introduction to the PeWEC underlying working principle, mooring, and associated mechanical system is presented within the following paragraphs.

The PeWEC is a floating offshore pendulum-based WEC, which harvests energy by means of the wave-induced pitch motion. Its working principle is outlined in Figure 1. The PeWEC pitch motion, excited by the incoming wave, induces a pendulum rotation around its axis (ε), which is connected, by means of a gearbox, to a PTO system.

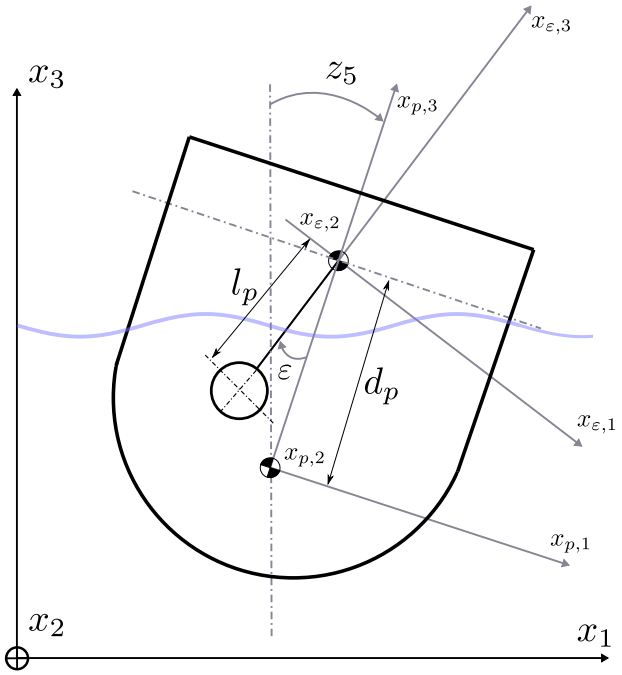

Figure 1. The PeWEC working principle in a schematic two-dimensional fashion.

Hull geometries and inertial properties are the result of an optimisation algorithm, which evaluates the device performance and minimises a corresponding cost function (i.e., capex over productivity) on a specific site. In particular, within this study, the PeWEC device has been optimised, taking into account the environmental conditions of Pantelleria (Sicily, Italy), by leveraging a genetic-based algorithm [25].

The PeWEC station-keeping problem is solved by adopting symmetrical spread mooring, formed by four catenary lines (see Figure 2), which are effectively "common" within the wave energy field [26,27]. Each line has a corresponding jumper attached to reduce the vertical load on the device and hence minimise any undesired effects on the device response.

A spread mooring system can significantly affect the harvested energy of a pitching device like the PeWEC, because it can restrain the weathervaning capabilities of the wave energy system. Moreover, Pantelleria represents a peculiar, environmentally speaking, site, because waves have a prevalent direction, as exposed in Figure 3. The PeWEC properties and the associated installation site data are both available in Table 1.

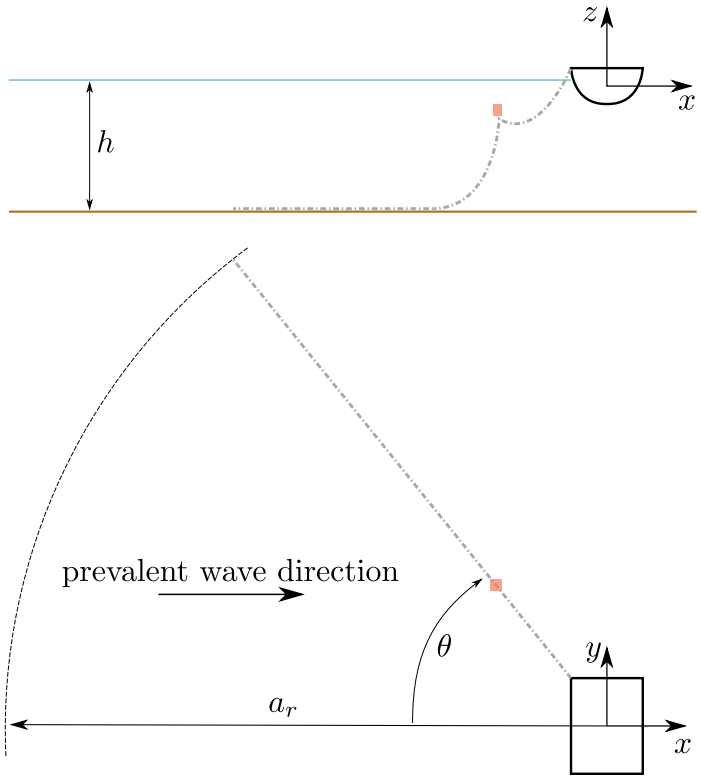

Figure 2. The PeWEC mooring system layout: schematic representation of one of the four catenary lines. Please note that, the sub-surface jumper is figured in red.

Table 1. PeWEC properties.

Property	Symbol	Unit	Value
Device properties			
device—mass	$m_{1,1}$	(kg)	$1.11 \cdot 10^7$
device—roll inertial moment	$m_{4,4}$	(kg·m^2)	$5.5 \cdot 10^7$
device—pitch inertial moment	$m_{5,5}$	(kg·m^2)	$3 \cdot 10^7$
device—yaw inertial moment	$m_{6,6}$	(kg·m^2)	$7.2 \cdot 10^7$
hydrostatic stiffness—heave	$h_{k,3,3}$	(N/m)	$3.1 \cdot 10^6$
hydrostatic stiffness—roll	$h_{k,4,4}$	(Nm/rad)	$1.2 \cdot 10^8$
hydrostatic stiffness—pitch	$h_{k,5,5}$	(Nm/rad)	$4 \cdot 10^7$
Pendulum properties			
pendulum—mass	m_p	(kg)	$7.17 \cdot 10^4$
pendulum—extent	d_p	(m)	2.44
pendulum—length	l_p	(m)	2.40
Site and mooring properties			
site water depth	w_d	(m)	38
mooring anchor radius	a_r	(m)	175
mooring line length	–	(m)	190
mooring line angle	θ	(deg)	60
chain nominal diameter	–	(mm)	80
chain axial stiffness	–	(N)	$546 \cdot 10^6$
chain linear mass	–	(kg/m)	127
jumper net buoyancy	–	(kg)	4000

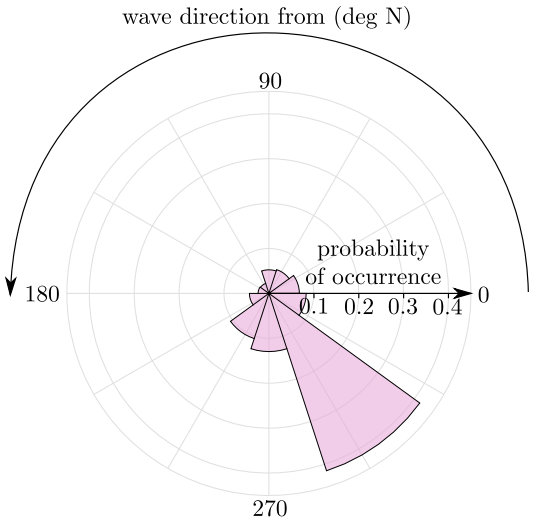

Figure 3. Rose diagram of the Pantelleria wave conditions: wave occurrences related to the coming-from direction.

3. Numerical Modelling

In this study, various numerical models are employed to capture the underlying system dynamics. While a frequency-domain approach can be utilised within linear assumptions (also by linearising nonlinear terms, see [28]), it is recognised that the use of a dynamic model is necessary when modelling a mooring system [29]. The following numerical models are employed in this study:

- Device hydrodynamics: The hydrodynamic effects acting on the device are incorporated using the assumptions corresponding with potential-flow theory [30]. Time-domain simulations are performed by computing the corresponding impulse response functions based on the well-known Cummins' equation [31].
- Mooring system: The mooring system is modelled using a dynamic lumped-mass model described in [32], and the numerical solver adopted is OrcaFlex (OF), being one of the most used in the offshore field [33]. External forces acting on the mooring system are included within the OF environment using the procedure proposed in [20].

Accordingly, the equation of motions of the device is

$$(m + m_\infty)\ddot{z}(t) + \int_{-\infty}^{t} h_r(\tau)\dot{z}(t-\tau)\mathrm{d}\tau + h_k z(t) = f_w(t) - f_{\mathrm{pend}}(t) - f_m(t), \qquad (1)$$

in which $\{m, m_\infty, h_k\} \subset \mathbb{R}^{6\times 6}$ represent the system inertia matrix, the so-called infinite-frequency added mass [31], and the hydrostatic stiffness, respectively. $\{f_w, f_{\mathrm{pend}}, f_m\} : \mathbb{R}^+ \to \mathbb{R}^6, t \mapsto \{f_w(t), f_{\mathrm{pend}}(t), f_m(t)\}$ are the wave exciting force, the pendulum reaction on the device, and the mooring restoring force, respectively. Finally, $h_r : \mathbb{R}^+ \to \mathbb{R}^{6\times 6}, t \mapsto h_r(t)$ represents the radiation impulse response function. Furthermore, it is possible to appreciate the integration of the following nonlinear terms:

- Wave force: The excitation force on the hull is evaluated by including the second-order terms (slow varying forces) defined in [34], precisely $f_w(t) = f_e(t) + f_{drift}(t)$, in which $f_{drift}(t)$ represents the drift forces acting on the device, given by the superposition of the mean drift forces and different-frequencies forces [34].
- Mooring force: The mooring problem is solved by means of OF as exposed in [32].
- Mechanism force: The integration of the mechanism and the associated control (the pendulum and the PTO) is achieved by means of an external library, following the approach proposed in [20]. The corresponding nonlinear equations are discussed within the following paragraph.

A graphical (schematic) representation of the equation of motion is presented in Figure 4. The pendulum equations are derived in a 3-DoFs model, by considering the surge, heave, and pitch motions. Note that the presented mathematical model, and its associated parameters, have been validated previously, see, e.g., [35,36]. The pendulum reaction on the hull, $f_{\text{pend}} : \mathbb{R} \to \mathbb{R}^6$, $t \mapsto f_{\text{pend}}(t)$, can be written as

$$\begin{aligned} f_{\text{pend}} &= [f_{\text{pend},1}, 0, f_{\text{pend},3}, 0, f_{\text{pend},5}, 0,]^\intercal, \\ f_{\text{pend},1} &= -m_p d_p \cos(z_5)\ddot{z}_5 - m_p l_p \cos(z_5+\varepsilon)(\ddot{z}_5+\ddot{\varepsilon}) \\ &+ m_p d_p \sin(z_5)\ddot{z}_5 - m_p l_p \sin(z_5+\varepsilon)(\dot{z}_5+\dot{\varepsilon})^2, \\ f_{\text{pend},3} &= m_p d_p \sin(z_5)\ddot{z}_5 - m_p l_p \sin(z_5+\varepsilon)(\ddot{z}_5+\ddot{\varepsilon}) \\ &+ m_p d_p \cos(z_5)\ddot{z}_5 - m_p l_p \cos(z_5+\varepsilon)(\dot{z}_5+\dot{\varepsilon})^2, \\ f_{\text{pend},5} &= f_{\text{ctrl}} + f_{\text{pend},1} d_p \cos(z_5) - f_{\text{pend},3} d_p \sin(z_5), \end{aligned} \tag{2}$$

where $\{m_p, l_p, d_p\} \subset \mathbb{R}^+$ represent the pendulum mass, pendulum length, and vertical extent between the pendulum fulcrum and the device centre of gravity (CoG), respectively. Moreover, $z_5 : \mathbb{R} \to \mathbb{R}$, $t \mapsto z_5(t)$ is the pitch motion, defined as the fifth entry of the device motion vector z, and $\varepsilon : \mathbb{R} \to \mathbb{R}$, $t \mapsto \varepsilon(t)$ is the rotation of the PTO axis. Finally, $f_{\text{ctrl}} : \mathbb{R} \to \mathbb{R}$, $t \mapsto f_{\text{ctrl}}(t)$ is the control torque applied to the PTO axis. The relation between the PeWEC pendulum rotation and its associated pitch motion can be described by the following equation:

$$\begin{aligned} &(m_{5,5} + m_p l_p^2)\ddot{\varepsilon} - m_p l_p \cos(z_5+\varepsilon)\ddot{z}_1 + m_p l_p \sin(z_5+\varepsilon)\ddot{z}_3 + \\ &(m_{5,5} + m_p l_p^2 - m_p d_p l_p \cos(\varepsilon))\ddot{z}_5 - m_p d_p l_p \sin(\varepsilon)\dot{z}_5^2 + \\ &m_p g l_p \sin(z_5+\varepsilon) + f_{\text{ctrl}} = 0, \end{aligned} \tag{3}$$

with $m_{5,5} \in \mathbb{R}^+$ the hull pitch inertial moment.

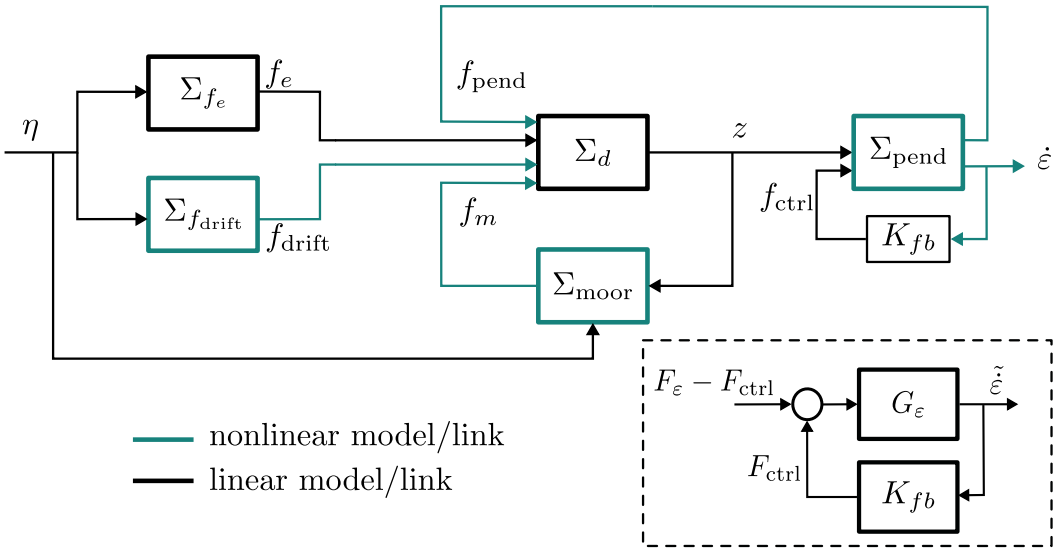

Figure 4. Schematic representation of the PeWEC system. The controlled system (under linear assumptions) is represented as the linear map G_ε.

As discussed previously in this section, the overall model experiences nonlinear actions, which are highlighted in Figure 4 using green lines. According to Cummins' Equation (1), it is possible to define the following subsystems: $\{\Sigma_{f_e}, \Sigma_{f_{\text{drift}}}\} : \mathbb{R} \to \mathbb{R}^6$, the linear and nonlinear maps related to the wave forces (f_e and f_{drift}, respectively); $\Sigma_{\text{moor}} : \mathbb{R}^6 \to \mathbb{R}^6$, the mooring nonlinear map; $\Sigma_{\text{pend}} : \mathbb{R}^6 \to \mathbb{R}^7$, the pendulum numerical representation; and, finally, $\Sigma_d : \mathbb{R}^6 \to \mathbb{R}^6$, the linear map associated to the device

hydrodynamics. Regarding the control action itself, $K_{fb} : \mathbb{R} \to \mathbb{R}$ represents the controller acting on the mechanical system.

Please note that, under linear assumptions, it is possible to represent the controlled system separately, in terms of an equivalent input/output map $G_\varepsilon : \mathbb{R} \to \mathbb{C}, \omega \mapsto G_\varepsilon(\omega)$ which defines the link between the total force acting on the PTO axis (F_ε) and the associated velocity ($\dot{\varepsilon}$).

We summarise, in the following, the main assumptions adopted within the mathematical modelling procedure:

- Hydrodynamics: The model is based on linear potential theory, which is expanded using nonlinear second-order forces. Linear potential models rely on the assumption of small motions and are generally unsuitable when excitation forces and device hydrodynamic properties (e.g., stiffness, among others) vary significantly. In most cases, this issue is limited to extreme wave scenarios [37], and the use of a linear potential-based model has already been validated for the PeWEC case [38].
- Mechanism: The model assumes that the pendulum effect primarily affects the pitch, surge, and heave motions. Note that the overall model is validated against experimental data in [36].
- Mooring: This model is based on a dynamic lumped-mass model, which effectively represents the state of the art in mooring modelling [33].

4. Control Synthesis for the PeWEC

As suggested in Paduano et al. [20], the control problem of the moored PeWEC can be faced by leveraging impedance-matching theory [39]. To keep this study reasonably self-contained, the description of the control synthesis and the associated theoretical background are briefly recalled. For a complete description, the interested reader is referred to [20,39–41].

4.1. Impedance-Matching Application

Figure 5 shows the PeWEC system under linear assumptions feedback-controlled in terms of the map $K_{fb}^{opt} : \mathbb{R} \to \mathbb{C}, s \mapsto K_{fb}^{opt}(s)$. The control action F_{ctrl}^{opt} can be interpreted in terms of an electric load, which needs to be designed with the objective of maximising the power extraction from the source, i.e., the force acting on the ε axis. Note that, as per the discussion provided previously within this section, $\dot{\varepsilon}$ represents the velocity of the PTO axis, and the map $G_\varepsilon : \mathbb{R} \to \mathbb{C}, s \mapsto G_\varepsilon(s)$ is the system to be controlled.

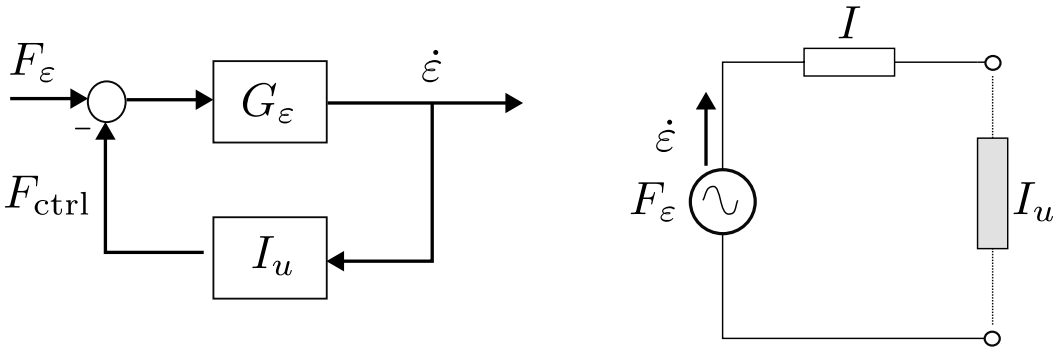

Figure 5. Impedance-matching principle: equivalent electrical circuit representation.

The resolution of this problem, under its electrical representation, can be addressed by means of the so-called impedance-matching theorem [42]. In particular, in order to maximise the power transfer, the load impedance K_{fb}^{opt} must be designed as the complex conjugate of the system impedance, which means, in the PeWEC case,

$$K_{fb}^{opt}(\omega) = I^*(\omega) = {G_\varepsilon}^{-*}(\omega). \tag{4}$$

The direct application of the condition in Equation (4), for every possible ω, cannot be achieved in practice due to the non-causality induced by the Hermitian operator (see [39]). To address this problem, it is possible to apply the impedance-matching principle by interpolating the optimal condition in (4) with an implementable (i.e., causal) controller structure on a matching frequency ω_m, i.e.,

$$K_{fb}(\omega_m) = K_{fb}^{opt}(\omega_m). \tag{5}$$

Though the choice of the interpolating frequency can be straightforward in monochromatic exciting conditions, when a panchromatic force excites the controlled system, the definition of ω_m is not trivial, compromising the performance of the adopted controller [39].

Therefore, in order to synthesise a suitable controller, the interpolating frequency can be selected by analysing, according to a given input wave spectrum, the spectrum of the exciting force $S_{f_\varepsilon} : \mathbb{R} \to \mathbb{R}^+, \omega \mapsto S_{f_\varepsilon}(\omega)$ [41]. To evaluate the force spectrum, the map $\tilde{\eta} : \mathbb{R} \to \mathbb{C}, \omega \mapsto \tilde{\eta}(\omega)$, which links the wave elevation with the total force acting on the PTO axis, can be leveraged.

As such, the uncontrolled system can be represented, under linear assumptions, as exposed in Figure 6. Finally, the spectrum of the exciting input acting on the PeWEC system can be defined as

$$S_{f_\varepsilon} = S_\eta G_{\eta 2 f_\varepsilon} G^*_{\eta 2 f_\varepsilon}, \tag{6}$$

in which $S_\eta : \mathbb{R} \to \mathbb{R}^+, \omega \mapsto S_\eta(\omega)$ represents the wave spectrum.

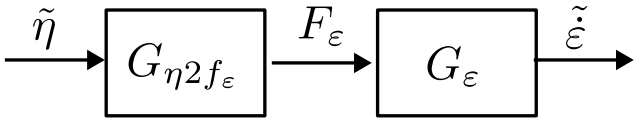

Figure 6. Identification of the pendulum axis excitation force.

4.2. Data-Based Modelling of the Controlled System

Bearing in mind the numerical tools available (see Section 3), it is clear that a significant limitation arises in the use of impedance-matching-based control synthesis, because most of the used models are nonlinear. This problem can be circumnavigated by leveraging a data-based model of the controlled system. The identification of the map G_ε, for the PeWEC case, is achieved by imposing a set of $N_j \in \mathbb{N}$ multisine input signals F^j_{ctrl} [43]. By applying this set of signals, it is straightforward to define the I/O empirical transfer function estimate for G_ε as

$$G_\varepsilon(\omega) = \sum_{j=1}^{N_j} \frac{1}{N_j} \frac{F^j_{\text{ctrl}}(\omega)}{\tilde{\varepsilon}^j(\omega)}, \tag{7}$$

where $\tilde{\varepsilon}^j$ denotes each output signal corresponding with the input F^j_{ctrl}.

The process described above is applied to the PeWEC-moored configuration so as to evaluate the corresponding frequency response map. In particular, this is exposed explicitly in Figure 7.

With the identified response (7), we proceed to synthesise an energy-maximising controller, following the impedance-matching theory presented in Section 4.1. In particular, the structure of the feedback controller adopted in this paper, which is used to interpolate the optimal impedance-matching response, is

$$K_{fb}(\omega) = \frac{k_\alpha \jmath\omega}{\jmath\omega + k_\beta}, \tag{8}$$

with $\{k_\alpha, k_\beta\} \subset \mathbb{R}$. Note that the proposed controller structure is an alternative of the classic proportional–integral (PI) controller, well known in the wave energy field. This

particular structure is adopted for the intrinsic stability condition that can be guaranteed in the controller closed-loop form, taking advantage of the WEC dissipativity property [44].

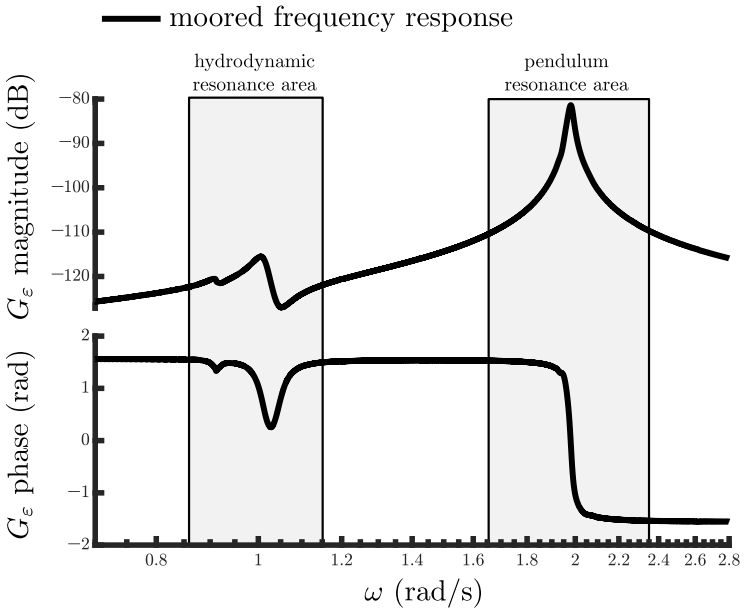

Figure 7. Averaged frequency responses (G_ε) for the moored and unmoored models.

Finally, it is possible to define, for a given interpolating frequency $\omega_m \in \mathbb{R}$, the control parameters for (8) as follows:

$$\begin{aligned} k_\alpha(\omega_m) &= \Re\left(\frac{1}{G_\varepsilon^*(\omega_m)}\right)\frac{\omega_m^2 + k_{\beta,m}^2}{\omega_m^2}, \\ k_\beta(\omega_m) &= \Im\left(\frac{1}{G_\varepsilon^*(\omega_m)}\right)\frac{\omega_m}{\Re\left(\frac{1}{G_\varepsilon^*(\omega_m)}\right)}. \end{aligned} \tag{9}$$

Within this study, irregular sea states are experienced by the pitching device, which means that the interpolating frequency can be achieved, as suggested in Section 4.1, by taking advantage of the map between the wave elevation and the PTO force, i.e., by identifying map $G_{\eta 2 f_\varepsilon}$ (see Figure 6), which can be achieved for a nonlinear system by computing the best linear approximation of the system [43]:

- Known wave spectra (i.e., Schroder phase multisine [43]) are simulated on the high fidelity model. For any simulation, the overall response is computed and averaged, i.e.,

$$G_\star = \frac{\tilde{\varepsilon}}{\tilde{\eta}}. \tag{10}$$

- The map $G_{\eta 2 f_\varepsilon}$ can be computed as

$$G_{\eta 2 f_\varepsilon} = \frac{G_\star}{G_\varepsilon}, \tag{11}$$

  with G_ε the frequency response evaluated as exposed in Section 4.
- The spectrum of the force on the ε axis can now be computed, i.e.,

$$S_{f_\varepsilon} = S_\eta\left(G_{\eta 2 f_\varepsilon} G_{\eta 2 f_\varepsilon}^*\right). \tag{12}$$

The map $G_{\eta 2 f_\varepsilon}$ is evaluated, and the associated amplitude is exposed in Figure 8. The system can be divided into two frequency regions, one defined by the device resonance (close to 1 rad/s) and one defined by the pendulum resonance (close to 2 rad/s). It can

be noticed that the output of the system $G_{\eta 2 f_\varepsilon}$ is more susceptible to exciting input with a frequency closer to the device resonance one. Once the force spectrum is computed, the matching frequency ω_m can be selected. Among the characteristic frequencies of the force exciting spectrum, within this study, the median is considered.

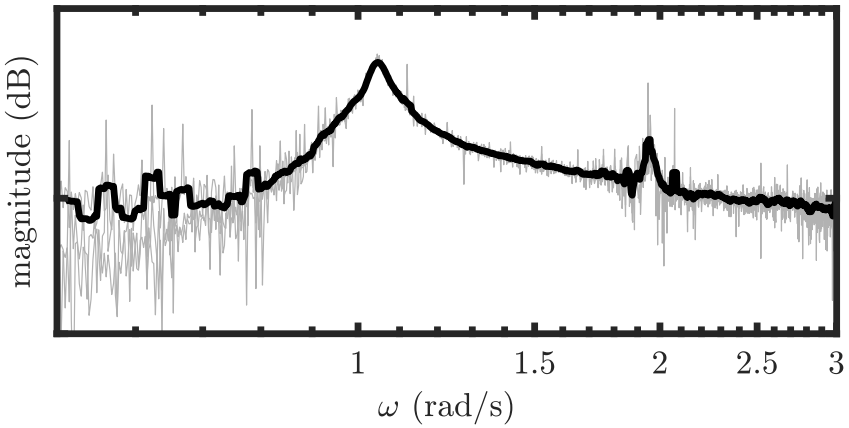

Figure 8. Identification of the $G_{\eta 2 f_\varepsilon}$ map. The averaged value of the several multisine signals is exposed in black.

5. Performance Assessment

The assessment of device productivity requires considering the performance across the entire scatter diagram of the site, which necessitates the inclusion of directionality. This aspect is particularly relevant for the PeWEC, as the device's ability to harvest energy is dependent on the incident wave direction. Including the directionality in the performance assessment of the PeWEC requires considerations on the deployment of the associated mooring system, because the orientation of the spread mooring (see Figure 2) will definitely impact the device performances. In the next paragraphs, the problem is faced by analysing a large set of environmental data in order to evaluate by means of a representative analysis the productivity of the PeWEC by analysing the directional scatter diagrams. The obtained productivity result is compared to the productivity achieved in an omnidirectional scenario. This comparison allows for the power loss resulting from the waves' directionality to be quantified and emphasises their significance in the overall performance assessment of the device.

To gather a comprehensive dataset, a total of 20 years' worth of hourly data are downloaded from the ERA5 online database [45]. This dataset serves as the foundation for the subsequent analysis. The downloaded data are utilised to investigate the distribution of the wave directions over the designated time period. This analysis provides valuable insights into the prevailing wave directions at the chosen site.

In Figure 9, the wave energy and occurrences (O_{en} and O_w, respectively) are represented as a function of the wave directionality. It can be noted that almost 70% of the site total energy is carried by waves coming from 300° N. Nevertheless, the waves from the same directions represent only 40% of the site conditions.

By leveraging the directionality characteristic of the site, and taking advantage of the device symmetry[1], the following steps can be followed in order to define and organise the site environmental conditions:

- Waves are divided into four main directions, which means four different scatters are built according to the direction between the waves and the device bow: $0 \pm 15°$, $30 \pm 15°$, $60 \pm 15°$, and $90 \pm 15°$.
- The 0° scatter is defined according to the most energetic directions (which actually is 300° N, see Figure 9).
- The bin size is set to 0.75 m and 0.75 s in order to define a representative set of waves.

- The waves simulated represent 95% of the site occurrence and 98% of the site energy: it means that most energetic waves on directional scatters are taken until 98% of the site energy and 95% of the site occurrence is reached[2].

According to the proposed discretisation, it is possible to minimise the number of simulated waves for non-prevalent directions. The scatters discretised according to the four main directions are reported in Appendix A.

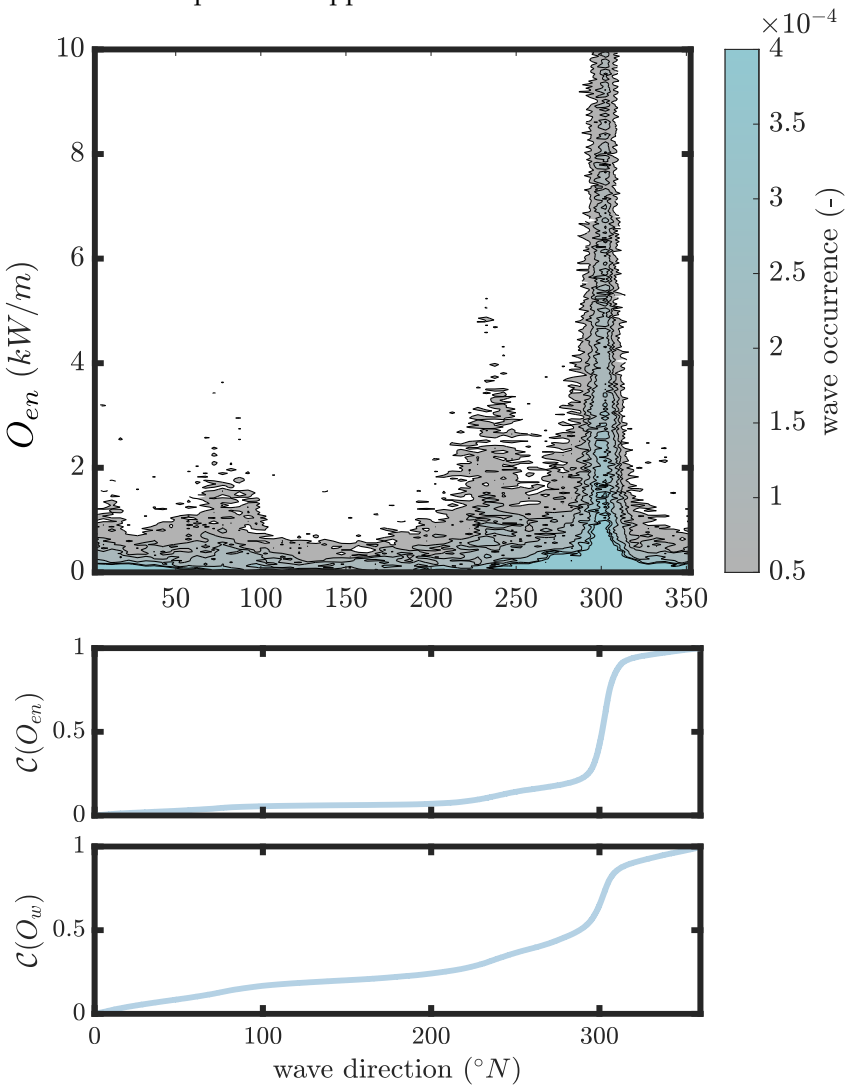

Figure 9. On top, wave energy and occurrences as a function of the wave directionality; on bottom, the cumulate of the wave energy and occurrence.

Once scatters are defined, a representative linear model of the moored system needs to be computed (such as the one exposed in Section 3). Please note that the directionality significantly influences the device response in the corresponding map $G_{\eta 2 f_\varepsilon}$. Therefore, by varying the directionality of the input signal $\tilde{\eta}$, it is possible to define the map $G_{\star,dd}$ (see Equation (11)), in which $dd \in [0, 30, 60, 90]$ represents the wave–bow orientation.

The maps of $G_{\eta 2 f_\varepsilon, dd}$ for different wave directions are shown in Figure 10. The influence of the wave direction on the equivalent force acting on the ε axis can be observed. The map associated with a 90°-oriented wave is not exactly zero due to the small yaw angles allowed by the mooring system. However, the force acting on the pendulum axis is lower than 30 dB when a wave comes from the side of the device, compared to a bow-oriented wave.

Based on this, the following simulations are conducted by omitting the 90° scatter.

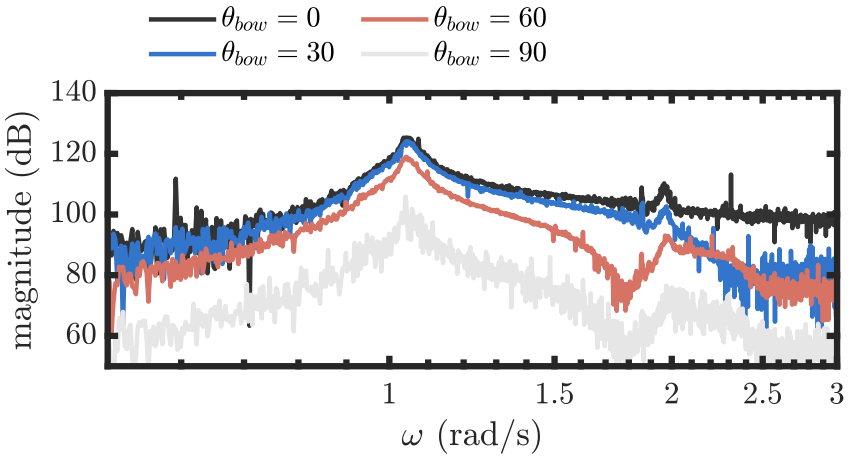

Figure 10. Identification of the $G_{\eta 2 f_\varepsilon}$ map for each direction.

Results

A total of 122 waves are simulated by means of the OF-based proposed tool.

Harvested mechanical energy is evaluated within the proposed case of study. The average mechanical power is calculated for a single wave condition as the mean of the instantaneous power, i.e.,

$$\mu_p = \frac{1}{N_k} \sum_{k=1}^{N_k} p_k(t), \tag{13}$$

in which $p : \mathbb{R} \to \mathbb{R}, t \mapsto p(t)$ is the instantaneous mechanical power evaluated as $p(t) = \dot{\epsilon}(t) f_{\text{ctrl}}(t)$. Consequently, the device power matrix, for each direction, is constructed by averaging the mechanical performance across all scenarios. The resultant power matrices are presented in Figure 11. Furthermore, Figure 12 illustrates the device response under one of the most energetic waves in the 0-degree scatter.

Once the device power matrices are available, the assessment of the overall productivity can be conducted by incorporating wave occurrences. This is achieved by multiplying the power matrix by the occurrences matrices, specifically for each direction:

$$\Gamma = N_{\text{hours}} \sum_{ii} \sum_{jj} \mu_{p,ii,jj} O_{w,ii,jj}, \tag{14}$$

where $N_{\text{hours}} \in \mathbb{N}$ represents the total number of hours in a year. The productivity is reported in Table 2.

Therefore, the productivity of the device on the Pantelleria site results in being equal to 46.8 $\frac{\text{MWh}}{\text{year}}$.

Omnidirectional Analysis

The omnidirectional productivity is evaluated to quantify the energy loss due to the monodirectional nature of the PeWEC. In this evaluation, it is assumed that all the waves at the site are directed towards the bow of the device. This allows for the definition of the omnidirectional scatter, which represents the overall performance of the device under these conditions.

Please note that the omnidirectional scatter is equivalent to the $\theta_{\text{bow}} = 0$ scatter in terms of the wave conditions. This means that the power matrix of the device is exactly the same in both cases, and the resulting productivity needs to be multiplied by the occurrences from the omnidirectional scatter.

The resulting productivity for the omnidirectional analysis results in being

$$\Gamma_{omni} = 70.3 \frac{\text{MWh}}{\text{year}}. \tag{15}$$

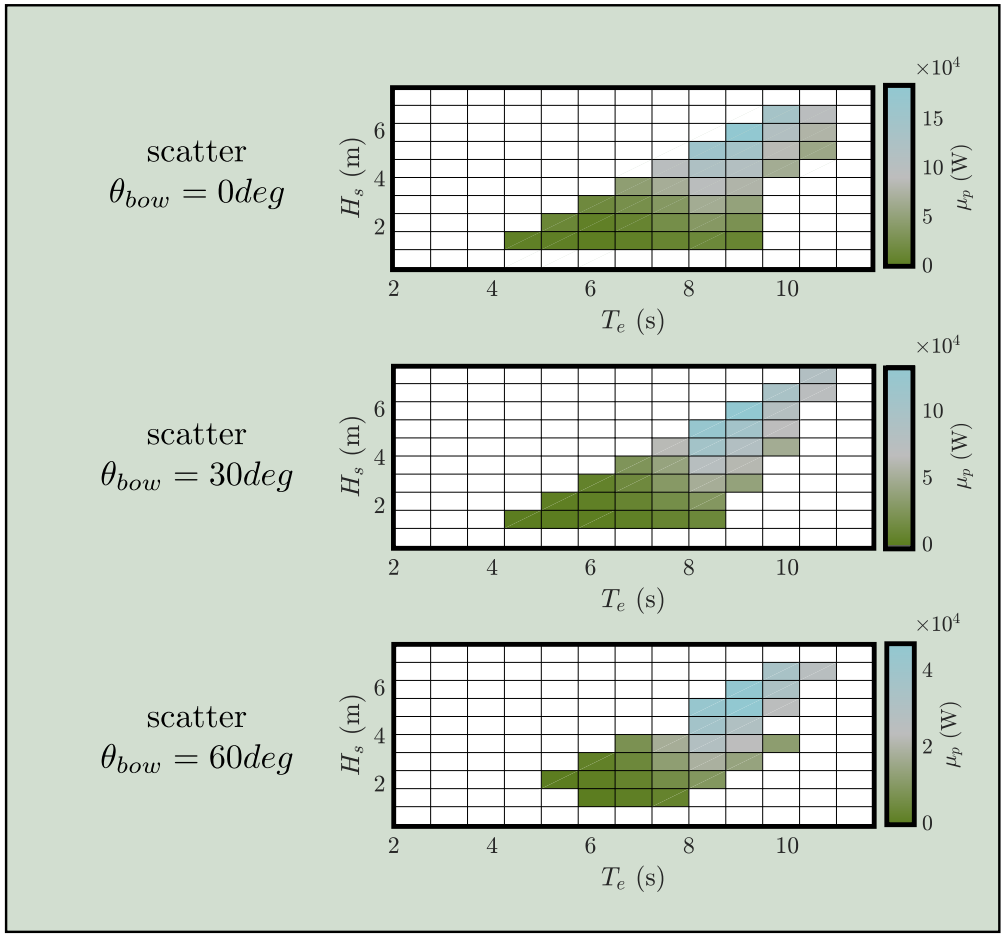

Figure 11. Directional power matrices for the moored PeWEC device.

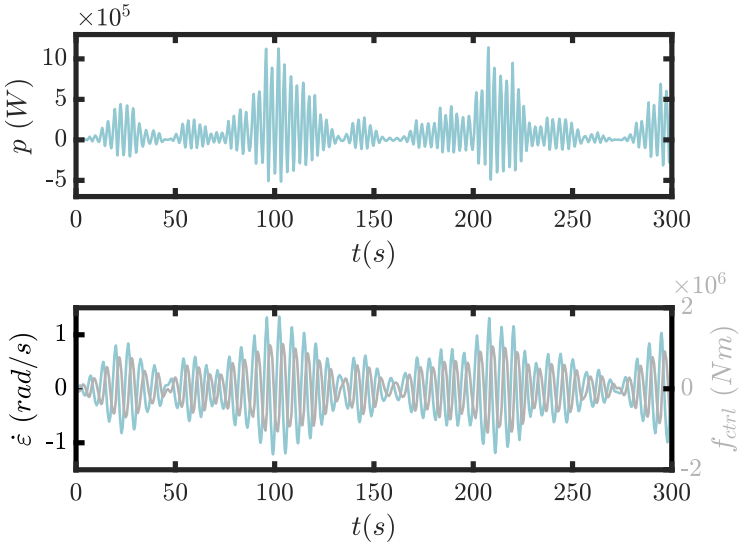

Figure 12. Device response when subject to a panchromatic wave condition, with the instantaneous power displayed at the top, and the PTO velocity $\dot{\varepsilon}$ (in blue) and control force f_{ctrl} (in grey) at the bottom. The wave spectrum is characterised by the following properties: $T_p = 6.5$ s, $H_s = 2.375$ m, and dir = 0 deg.

Table 2. Device productivity.

$\theta_{\mathbf{bow}}$ (°)	Γ ($\frac{\mathbf{MWh}}{\mathbf{year}}$)
0	31.7
30	11.4
60	3.7

The analysis of the omnidirectional productivity reveals that the PeWEC overall energy extraction capability is reduced by 34% due to the waves' directionality at the Pantelleria site. This finding highlights the significant impact that wave direction can have on the performance of the device. Despite the PeWEC's ability to harvest energy from stern-coming waves as well as bow-coming waves, the loss of energy due to the restricted wave approach direction is significant. For the sake of completeness, the device capture width ratio (CWR) is evaluated on the overall 0 deg scatter, exposed in Figure 13. The CWR, also called hydrodynamic efficiency [46], expresses the fraction of the wave power absorbed by the device, i.e.,

$$\mathrm{CWR} = 100\frac{\mu_p}{O_{en}B}, \tag{16}$$

in which $B = 22.5$ m represents the device width.

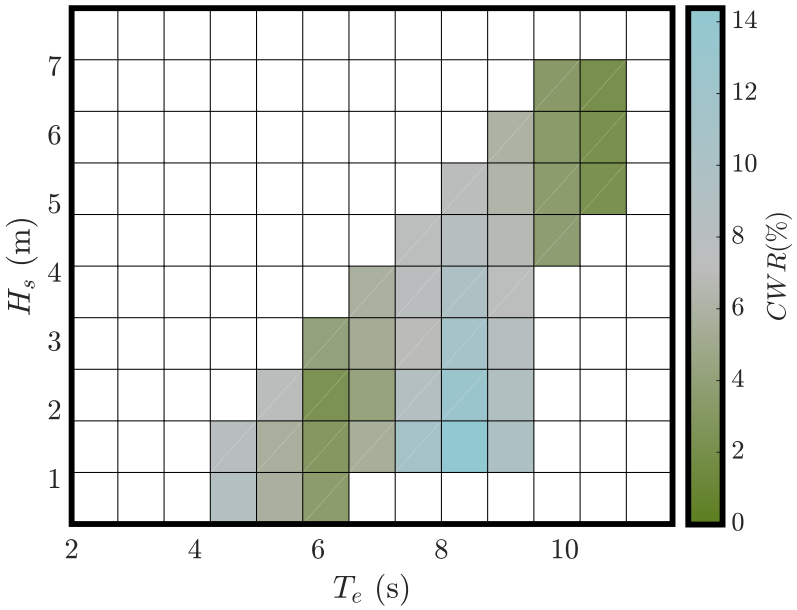

Figure 13. Device CWR 0 deg scatter.

Please note that the CWR of the PeWEC is consistent with that of other point-absorber devices [46].

6. Conclusions

Moorings influence WEC performances by affecting the overall motion and restraining the device's weathervaning capability. Although the first problem is analysed in the state of the art [20], the inclusion of the wave directionality within the control synthesis and performance assessment of a moored device still results in being a novelty. This study aims to address this problem by analysing the PeWEC representative case study, because its performances can be influenced by the waves' direction.

Site environmental conditions are pre-processed in order to define a comprehensive set of waves, defined in four directional scatter diagrams. The problem of the control synthesis

is then addressed including the wave directionality and, consequently, performances of the moored PeWEC on the directional scatters are evaluated. Finally, the omnidirectional conditions are compared in terms of productivity to remark on the importance of directionality in the device performance assessment.

Although the site conditions result in having a prevalent wave direction, by neglecting the directionality problem for the PeWEC case study, device performances can be overestimated up to 50%. To synthesise, because a significant part of wave energy systems can be influenced by the wave directionality [12], such information needs to be included in the system design stage in order to provide reliable results.

While the control action synthesised using impedance-matching theory has limitations in practical applications, such as the absence of inherent constraint handling, this study emphasises the importance of assessing WEC performance comprehensively, even when analysing sites with prevalent wave directions. It is worth noting that the significant dynamics of the mooring system can be incorporated by linearising mooring actions to synthesise controllers using numerical techniques [22]. Furthermore, although the optimal control action remains unaffected by wave directions in unconstrained conditions, the inclusion of a mooring system can also influence the synthesised controller, also when considering heaving devices [21]. In general, to pave the way for the commercialisation of wave energy systems, careful consideration of the mooring system and wave directionality should be performed in the initial optimisation stages of device development. This study focuses on addressing the current challenges in wave energy system modelling to advance representative holistic optimisation strategies.

Author Contributions: Conceptualization, B.P. and G.M.; Methodology, B.P. and N.F.; Investigation, B.P.; Writing—original draft, B.P.; Writing—review & editing, B.P. and N.F.; Supervision, N.F. and G.M. All authors have read and agreed to the published version of the manuscript.

Funding: This research received no external funding.

Data Availability Statement: Not applicable.

Conflicts of Interest: The authors declare no conflict of interest.

Appendix A

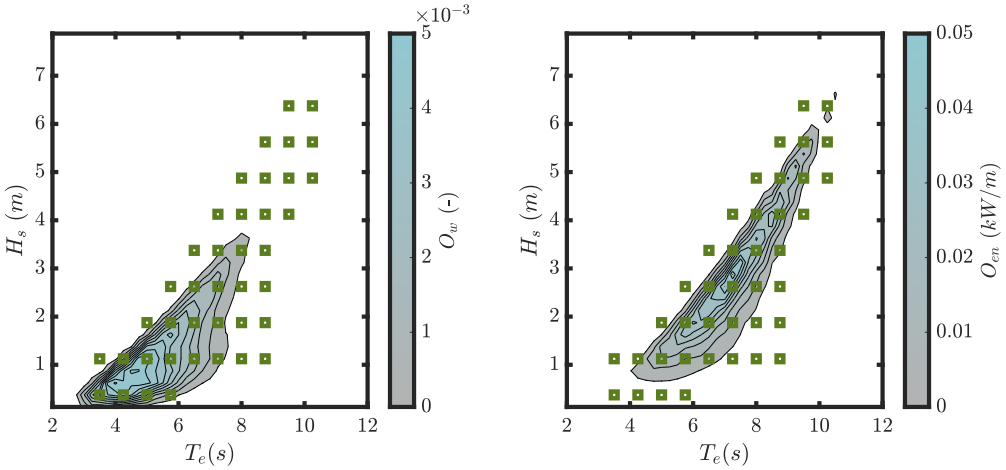

Figure A1. Wave directional scatter for the Pantelleria site, Italy. Occurrences scatter on the left, and energetic scatter on the right. The scatter is defined according to the wave directionality of 0° to the device's bow, and the chosen waves are represented with green square markers.

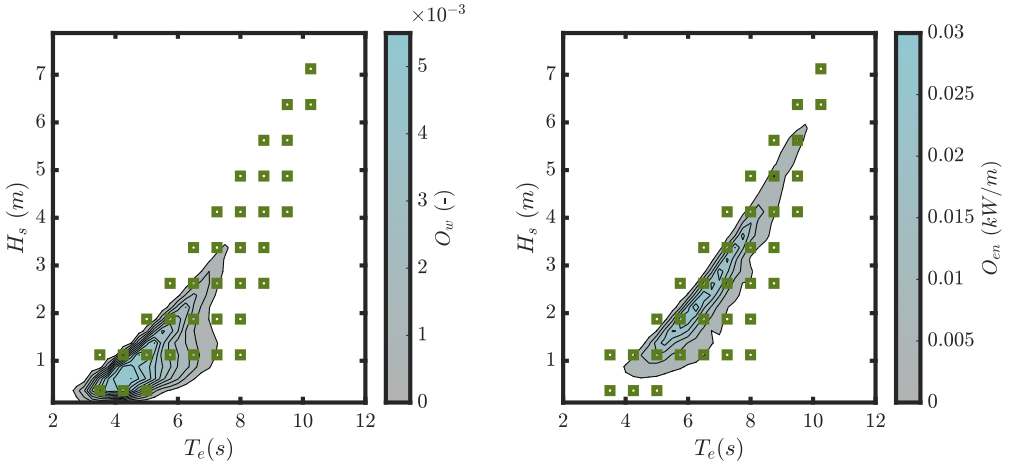

Figure A2. Wave directional scatter for the Pantelleria site, Italy. Occurrences scatter on the left, and energetic scatter on the right. The scatter is defined according to the wave directionality of 30° to the device's bow, and the chosen waves are represented with green square markers.

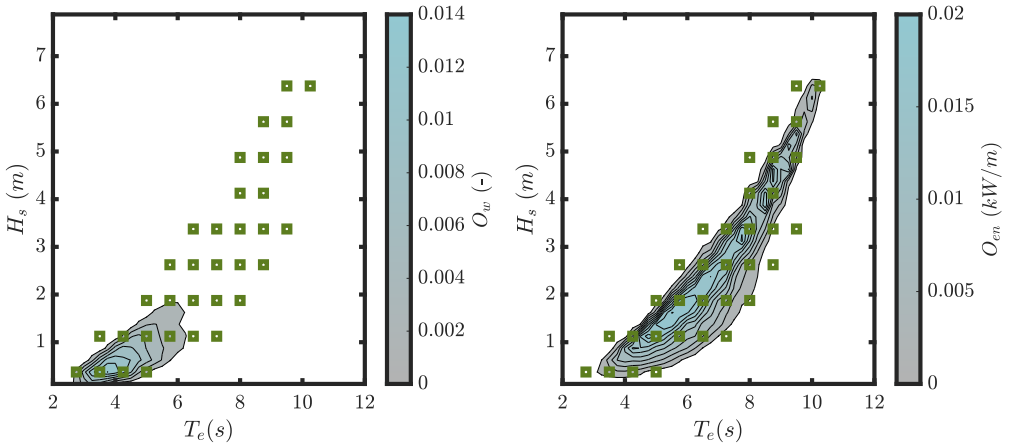

Figure A3. Wave directional scatter for the Pantelleria site, Italy. Occurrences scatter on the left, and energetic scatter on the right. The scatter is defined according to the wave directionality of 60° ± 15° according to the device's bow, and the chosen waves are represented with green square markers.

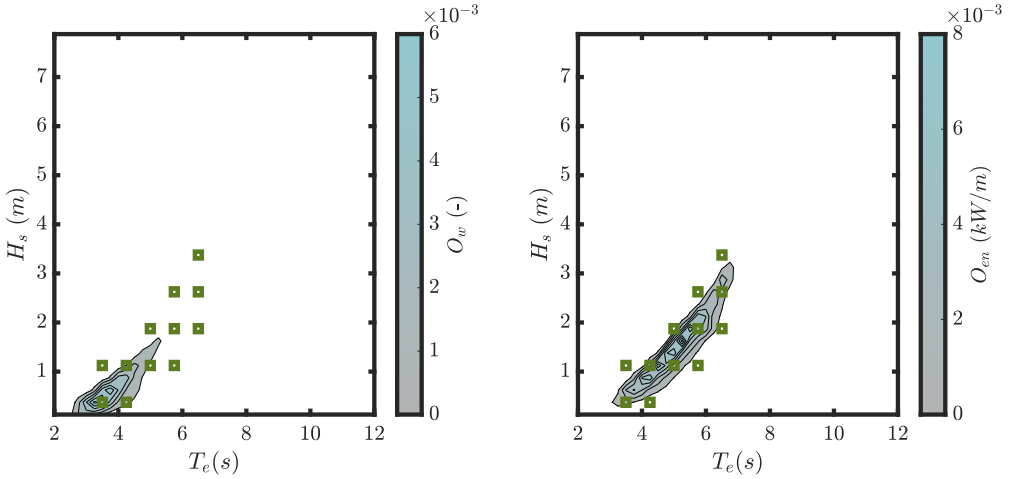

Figure A4. Wave directional scatter for the Pantelleria site, Italy. Occurrences scatter on the left, and energetic scatter on the right. The scatter is defined according to the wave directionality of 90° to the device's bow, and the chosen waves are represented with green square markers.

Notes

[1] The PeWEC takes advantage of a double symmetry. It is able to harvest energy from stern-coming waves, such as the bow-coming ones.

[2] Please note that cutting off 2% of the total energy and 5% of the total occurrences halves the number of waves.

References

1. Thorpe, T.W. A Brief Review of Wave Energy Harwell Laboratory, Energy Technology Support Unit, 1999. Available online: https://books.google.com/books/about/A_Brief_Review_of_Wave_Energy.html?id=9NeZswEACAAJ (accessed on 11 October 2023).
2. Ilyas, A.; Kashif, S.A.; Saqib, M.A.; Asad, M.M. Wave electrical energy systems: Implementation, challenges and environmental issues. *Renew. Sustain. Energy Rev.* **2014**, *40*, 260–268. [CrossRef]
3. Aderinto, T.; Li, H. Ocean Wave energy converters: Status and challenges. *Energies* **2018**, *11*, 1250. [CrossRef]
4. Sasaki, K. Ocean wave energy: current status and future perspectives. *J. Soc. Mech. Eng.* **2008**, *45*, 45–6810. [CrossRef]
5. Cruz, J. *Ocean Wave Energy: Current Status and Future Prespectives*; Springer: Berlin/Heidelberg, Germany, 2008. [CrossRef]
6. Lehmann, M.; Karimpour, F.; Goudey, C.A.; Jacobson, P.T.; Alam, M.R. Ocean wave energy in the United States: Current status and future perspectives. *Renew. Sustain. Energy Rev.* **2017**, *74*, 1300–1313. [CrossRef]
7. Mustapa, M.A.; Yaakob, O.B.; Ahmed, Y.M.; Rheem, C.K.; Koh, K.K.; Adnan, F.A. Wave energy device and breakwater integration: A review. *Renew. Sustain. Energy Rev.* **2017**, *77*, 43–58. [CrossRef]
8. Wahyudie, A.; Jama, M.A.; Susilo, T.B.; Saeed, O.; Nandar, C.S.; Harib, K. Simple bottom-up hierarchical control strategy for heaving wave energy converters. *Int. J. Electr. Power Energy Syst.* **2017**, *87*, 211–221. [CrossRef]
9. Mørk, G.; Barstow, S.; Kabuth, A.; Pontes, M.T. Assessing the global wave energy potential. *Proc. Int. Conf. Offshore Mech. Arct. Eng.-OMAE* **2010**, *3*, 447–454. [CrossRef]
10. European Commission. Energy Rodmap 2050, Impact Assessment and Scenario Analysis. Brussels, 2011. Available online: https://energy.ec.europa.eu/system/files/2014-10/roadmap2050_ia_20120430_en_0.pdf (accessed on 11 October 2023).
11. World Meteorological Organization. *Guide to Wave Analysis and Forecasting*; Secretariat of the World Meteorological Organization: Geneva, Switzerland, 1988; ISBN 92-63-12702-6.
12. Czech, B.; Bauer, P. Wave Energy Converter Concepts: Design Challenges and Classification. *IEEE Ind. Electron. Mag.* **2012**, *6*, 4–16. [CrossRef]
13. Faedo, N. Optimal Control and Model Reduction for Wave Energy Systems: A Moment-Based Approach. Ph.D. Thesis, Maynooth University, Maynooth, Ireland, 2020. Available online: https://mural.maynoothuniversity.ie/13541/ (accessed on 11 October 2023).
14. Pasta, E.; Faedo, N.; Mattiazzo, G.; Ringwood, J. Towards data-driven and data-based control of wave energy systems: Classification, overview, and critical assessment. *Renew. Sustain. Energy Rev.* **2023**, 188, 113877. [CrossRef]
15. Bhinder, M.; Karimirad, M.; Weller, S.; Debruyne, Y.; Guerinel, M.; Sheng, W. Modelling mooring line non-linearities (material and geometric effects) for a wave energy converter using AQWA, SIMA and Orcaflex. In Proceedings of the 11th European Wave and Tidal Energy Conference (EWTEC 2015), Nantes, France, 6–11 September 2015. Available online: https://tethys-engineering.pnnl.gov/publications/modelling-mooring-line-non-linearities-material-geometric-effects-wave-energy (accessed on 11 October 2023).
16. Depalo, F.; Wang, S.; Xu, S.; Soares, C.G. Design and analysis of a mooring system for a wave energy converter. *J. Mar. Sci. Eng.* **2021**, *9*, 782. [CrossRef]
17. Mao, Y.; Wang, T.; Duan, M. A DNN-based approach to predict dynamic mooring tensions for semi-submersible platform under a mooring line failure condition. *Ocean. Eng.* **2022**, *266*, 112767. [CrossRef]
18. Wei, H.; Xiao, L.; Liu, M.; Kou, Y. Data-driven model and key features based on supervised learning for truncation design of mooring and riser system. *Ocean. Eng.* **2021**, *224*, 108743. [CrossRef]
19. Paduano, B.; Pasta, E.; Papini, G.; Carapellese, F.; Bracco, G. Mooring Influence on the Productivity of a Pitching Wave Energy Converter. In Proceedings of the OCEANS 2021, San Diego, CA, USA, 20–23 September 2021 ; pp. 1–6. [CrossRef]
20. Paduano, B.; Carapellese, F.; Pasta, E.; Sergej, S.; Faedo, N.; Mattiazzo, G. Data-based control synthesis and performance assessment for moored wave energy conversion systems: The PeWEC case. *IEEE Trans. Sustain. Energy* **2023**, 1–12. [CrossRef]
21. Paduano, B.; Pasta, E.; Carapellese, F.; Papini, G.; Baltazar, J.; Faedo, N.; Mattiazzo, G. Control co-design mooring optimisation for wave energy systems: a three-tethered point absorber case. In Proceedings of the IFAC World Congress, Yokohama, Japan, 9–14 July 2023.
22. Papini, G.; Paduano, B.; Pasta, E.; Carapellese, F.; Mattiazzo, G.; Faedo, N. On the influence of mooring systems in optimal predictive control for wave energy converters. *Renew. Energy* **2023**, *218*, 119242. [CrossRef]
23. Carapellese, F.; Pasta, E.; Faedo, N.; Giorgi, G. Dynamic analysis and performance assessment of the Inertial Sea Wave Energy Converter (ISWEC) device via harmonic balance. *IFAC-PapersOnLine* **2022**, *55*, 439–444. [CrossRef]
24. Rusu, L.; Onea, F. Assessment of the performances of various wave energy converters along the European continental coasts. *Energy* **2015**, *82*, 889–904. [CrossRef]
25. Sirigu, S.A.; Foglietta, L.; Giorgi, G.; Bonfanti, M.; Cervelli, G.; Bracco, G.; Mattiazzo, G. Techno-Economic Optimisation for a Wave Energy Converter via Genetic Algorithm. *J. Mar. Sci. Eng.* **2020**, *8*, 482. [CrossRef]

26. Harris, R.; Johanning, L.; Wolfram, J. Mooring systems for wave energy converters: A review of design issues and choices. *PRoceedings Inst. Mech. Eng. Part B J. Eng. Manuf.* **2006**, *220*, 159–168.
27. Qiao, D.; Haider, R.; Yan, J.; Ning, D.; Li, B. Review of wave energy converter and design of mooring system. *Sustainability* **2020**, *12*, 8251. [CrossRef]
28. Bonfanti, M.; Giorgi, G. Improving Computational Efficiency in WEC Design: Spectral-Domain Modelling in Techno-Economic Optimization. *J. Mar. Sci. Eng.* **2022**, *10*, 1468. [CrossRef]
29. Paduano, B.; Carapellese, F.; Pasta, E.; Faedo, N.; Mattiazzo, G. Optimal controller tuning for a nonlinear moored wave energy converter via non-parametric frequency-domain techniques. In *Trends in Renewable Energies Offshore*, 1st ed.; CRC Press: Boca Raton, FL, USA, 2022; 8p. [CrossRef]
30. Journee, J.M.J.; Massie, W.W. *Offshore Hydromechanics*, 1st ed.; Delft University of Technology: Delft, The Netherland, 2001.
31. Cummins, W.E. The Impulse Response Function and Ship Motions. *Schiffstechnik* **1962**, *9*, 101–109.
32. Orcina. *OrcaFlex Manual*; Orcina Ltd.: Ulverston, UK, 2020. Available online: https://www.orcina.com/webhelp/OrcaFlex/ (accessed on 11 October 2023).
33. Davidson, J.; Ringwood, J.V. Mathematical modelling of mooring systems for wave energy converters—A review. *Energies* **2017**, *10*, 666. [CrossRef]
34. Faltinsen, O. *Sea Loads on Ships and Offshore Structures*; Cambridge University Press: Cambridge, UK, 1993.
35. Pozzi, N.; Bonfanti, M.; Mattiazzo, G. Mathematical Modeling and Scaling of the Friction Losses of a Mechanical Gyroscope. *Int. J. Appl. Mech.* **2018**, *10*. [CrossRef]
36. Pozzi, N.; Bracco, G.; Passione, B.; Sirigu, S.A.; Mattiazzo, G. PeWEC: Experimental validation of wave to PTO numerical model. *Ocean. Eng.* **2018**, *167*, 114–129. [CrossRef]
37. Penalba, M.; Giorgi, G.; Ringwood, J.V. Mathematical modelling of wave energy converters: a review of nonlinear approaches. *Renew. Sustain. Energy Rev.* **2017**, *78*, 1188–1207. [CrossRef]
38. Niosi, F.; Begovic, E.; Bertorello, C.; Rinauro, B.; Sannino, G.; Bonfanti, M.; Sirigu, S.A. Experimental validation of Orcaflex-based numerical models for the PEWEC device. *Ocean. Eng.* **2023**, *281*, 114963. [CrossRef]
39. Faedo, N.; Carapellese, F.; Pasta, E.; Mattiazzo, G. On the principle of impedance-matching for underactuated wave energy harvesting systems. *Appl. Ocean. Res.* **2022**, *118*, 102958. [CrossRef]
40. Carapellese, F.; Pasta, E.; Paduano, B.; Faedo, N.; Mattiazzo, G. Intuitive LTI energy-maximising control for multi-degree of freedom wave energy converters: the PeWEC case. *Ocean. Eng.* **2022**, 256, 111444. [CrossRef]
41. Paduano, B.; Edoardo, P.; Faedo, N.; Mattiazzo, G. Control synthesis via Impedance-Matching in panchromatic conditions: A generalised framework for moored systems. In Proceedings of the European Wave and Tidal Energy Conference, Bilbao, Spain, 3–7 September 2023; Volume 15. [CrossRef]
42. Floyd, T.L.; Pownell, E. *Principles of Electric Circuits: Conventional Current*; Pearson Education, 2021. Available online: https://books.google.com/books?id=KskQzgEACAAJ (accessed on 11 October 2023).
43. Pintelon, R.; Schoukens, J. *System Identification: A Frequency Domain Approach*, 2nd ed.; Wiley: Hoboken, NJ, USA, 2012; pp. 1–787.
44. Faedo, N.; Peña-Sanchez, Y.; Carapellese, F.; Mattiazzo, G.; Ringwood, J.V. LMI-based passivation of LTI systems with application to marine structures. *IET Renew. Power Gener.* **2021**, *15*, 3424–3433. [CrossRef]
45. Hersbach, H.; Bell, B.; Berrisford, P.; Hirahara, S.; Horányi, A.; Muñoz-Sabater, J.; Nicolas, J.; Peubey, C.; Radu, R.; Schepers, D.; et al. The ERA5 global reanalysis. *Q. J. R. Meteorol. Soc.* **2020**, *146*, 1999–2049. [CrossRef]
46. Babarit, A. A database of capture width ratio of wave energy converters. *Renew. Energy* **2015**, *80*, 610–628. [CrossRef]